

1
2
3
4
5 Capacitance of Two-Dimensional Titanium Carbide
6
7
8
9 (MXene) and MXene/Carbon Nanotube Composites
10
11
12
13
14 in Organic Electrolytes
15
16
17

18 *Yohan Dall'Agnese^{1,2,3}, Patrick Rozier^{1,2}, Pierre-Louis Taberna^{1,2}, Yury Gogotsi³,*
19
20 *Patrice Simon^{1,2*}*

21
22
23
24 ¹ Université Paul Sabatier, CIRIMAT UMR CNRS 5085, 118 route de Narbonne, 31062
25
26
27 Toulouse, France

28
29
30 ² Réseau sur le Stockage Electrochimique de l'Energie (RS2E), FR CNRS 3459, France
31
32

33
34 ³ Department of Materials Science and Engineering, and A. J. Drexel Nanomaterials Institute,
35
36
37 Drexel University, Philadelphia, PA 19104, USA
38
39
40
41
42

43 **Corresponding Author**

44
45
46 * Email: simon@chimie.ups-tlse.fr
47
48

49 Tel: +33(0)5.61.55.68.02
50
51
52
53
54
55
56
57
58
59
60
61
62
63
64
65

1
2
3
4 **Abstract**
5

6 Pseudocapacitive materials that store charges by fast redox reactions are promising candidates
7 for designing high energy density electrochemical capacitors. MXenes - recently discovered two-
8 dimensional carbides, have shown excellent capacitance in aqueous electrolytes, but in a narrow
9 potential window, which limits both the energy and power density. Here, we investigated the
10 electrochemical behavior of Ti_3C_2 MXene in 1M solution of 1-ethyl-3-methylimidazolium bis-
11 (trifluoromethylsulfonyl)-imide (EMITFSI) in acetonitrile and two other common organic
12 electrolytes. This paper describes the use of clay, delaminated and composite Ti_3C_2 electrodes
13 with carbon nanotubes in order to understand the effect of the electrode architecture and
14 composition on the electrochemical performance. Capacitance values of $85 F g^{-1}$ and $245 F cm^{-3}$
15 were obtained at $2 mV s^{-1}$, with a high rate capability and good cyclability. *In situ* X-ray
16 diffraction study reveals the intercalation of large EMI^+ cations into MXene, which leads to
17 increased capacitance, but may also be the rate limiting factor that determines the device
18 performance.
19
20
21
22
23
24
25
26
27
28
29
30
31
32
33
34
35
36
37
38

39 **KEYWORDS**
40

41
42 Electrochemical capacitors; two-dimensional materials; MXene; X-ray diffraction; carbon
43 nanotube, titanium carbide
44
45
46
47
48
49
50
51
52
53
54
55
56
57
58
59
60
61
62
63
64
65

1. Introduction

Electrochemical capacitors (ECs) are commercial devices used for high power delivery applications [1, 2]. They typically utilize either porous carbon materials or pseudocapacitive materials for electrostatic or redox energy storage, respectively [3, 4]. In the latter, the charge is stored by fast redox reactions at the surface of materials such as MnO_2 , RuO_2 , Nb_2O_5 or MoO_3 [5-8]. Recently, energy storage based on ion intercalation into two-dimensional (2D) materials has attracted much attention because of promising results with up to 375 F g^{-1} in KOH or 200 F g^{-1} in organic electrolyte for functionalized graphene [9, 10].

A new family of two-dimensional materials called MXenes has emerged as promising electrodes for energy storage devices such as batteries [11-15], metal ion (Li^+ , Na^+) capacitors [16-18] and ECs [19-22]. MXenes are synthesized by selective etching of the A layer from the conductive ternary carbide family of MAX phases [23]. Of the MXene family, Ti_3C_2 was the first discovered and is the most studied to date. First studies of Ti_3C_2 as electrode material in supercapacitors showed capacities up to 100 F g^{-1} for intercalation of cations such as Li^+ , Mg^{2+} or Al^{3+} in aqueous electrolytes [19]. Aside, MXene performance can be greatly improved by tuning the surface functional groups, delamination or addition of carbon nanoparticles [14, 21, 22]. Delaminated Ti_3C_2 electrodes containing carbon nanotubes have also shown noteworthy performance in lithium ion batteries, as well as in aqueous supercapacitors with capacity up to 430 mAh g^{-1} and capacitance of 140 F g^{-1} , respectively [14, 22]. The modification of the chemistry of the surface groups through a new “clay” synthesis route led to a 2-fold increase in volumetric capacitance (up to 900 F cm^{-3}) in sulfuric acid electrolyte due to dense packing of 2D MXene sheets combined with their accessibility due to pre-intercalation of ions during the

1
2
3
4 synthesis [20]. The role of pseudocapacitance in these high values was confirmed by showing a
5
6 reversible change in the oxidation state of titanium atoms in MXene [24].
7
8

9 However, MXene has been investigated as electrode material for ECs mainly in aqueous
10 electrolytes, which show a limited potential window due to water electrolysis. Moreover,
11 oxidation of Ti_3C_2 under high anodic potentials in aqueous electrolytes further limits its use to
12 cathodes of asymmetric devices. As both the energy and the power density increase with the
13 square of the potential window, its expansion is one of the key challenges for designing SCs with
14 improved performance and organic electrolyte may expand the voltage window beyond 2-2.5 V.
15
16
17
18
19
20
21
22

23 In this work, we report on the electrochemical performance of Ti_3C_2 in organic supercapacitor
24 electrolytes for supercapacitor applications. The energy storage mechanism was studied by *in*
25
26
27
28
29 *situ* X-ray diffraction (XRD).
30
31
32

33 **2. Experimental**

34 **2.1 Electrode preparation**

35
36
37
38 Ti_3C_2 was synthesized by selectively etching the aluminum layer out of the Ti_3AlC_2 MAX
39 phase in a 6M HCl/LiF solution at 35°C for 24h [20]. The obtained material was then washed
40 with distilled water. MXene samples after synthesis were terminated with OH, O and F and we
41 add T_x to the Ti_3C_2 formula to show those surface terminations. Full delamination of $Ti_3C_2T_x$
42 was obtained by ultrasonication for 1h in distilled water. A composite material was prepared by
43 mixing the colloidal solution of delaminated Ti_3C_2 with 20 wt. % of multiwalled carbon
44 nanotubes (MWCNT C100, Graphistrength) which have specific surface area of 175 m² g⁻¹. The
45 as-synthesized $Ti_3C_2T_x$, the delaminated $Ti_3C_2T_x$ and the CNT/ $Ti_3C_2T_x$ composite were filtered
46
47
48
49
50
51
52
53
54
55
56
57
58 on polypropylene membranes then rolled into film electrodes on Teflon membranes using a glass
59
60
61
62
63
64
65

1
2
3
4 tube. Once dried, the films were easily removed from the membrane to obtain the freestanding
5
6 $\text{Ti}_3\text{C}_2\text{T}_x$, d- $\text{Ti}_3\text{C}_2\text{T}_x$ and CNT- $\text{Ti}_3\text{C}_2\text{T}_x$ films without binder. The electrodes were prepared by
7
8 cutting the films into $\sim 25 \text{ mm}^2$ rectangles with a razor blade. The thicknesses were measured
9
10 from scanning electron microscope observations and $\text{Ti}_3\text{C}_2\text{T}_x$, d- $\text{Ti}_3\text{C}_2\text{T}_x$ and CNT- $\text{Ti}_3\text{C}_2\text{T}_x$ film
11
12 densities were calculated to be 2.3 g cm^{-3} , 3.0 g cm^{-3} and 2.9 g cm^{-3} , respectively.
13
14
15

16 **2.2 Electrochemical testing**

17
18
19 Three-electrode Swagelok© cells were used with Ti_3C_2 as working electrode, an Ag wire as a
20
21 pseudo-reference electrode and a commercial activated carbon (YP17 Kuraray, Japan)
22
23 overcapacitive counter electrode prepared by mixing 5 wt.% polytetrafluoroethylene binder (60
24
25 wt.% in H_2O , Aldrich) to 95 wt.% of YP17. A polypropylene membrane (GH Polypro, Pall) was
26
27 used as a separator. The electrolyte was a 1 M solution of EMITFSI (1-ethyl-3-
28
29 methylimidazolium bis(trifluoromethylsulfonyl)imide, Solvionic) in acetonitrile (Acros
30
31 Organics). For comparison purposes, 1 M EMIBF₄ (1-ethyl-3-methylimidazolium
32
33 tetrafluoroborate, Fluka) and 1 M TEABF₄ (tetraethylammonium tetrafluoroborate, Acros
34
35 Organics) in acetonitrile were tested. The cells were assembled in an argon-filled glovebox. A
36
37 VMP3 potentiostat (Biologic SA, France) was used for electrochemical testing. Cyclic
38
39 voltammetry (CV) was performed at scan rate from 2 to 100 mV s^{-1} ; capacitance values were
40
41 calculated by integrating the reduction current. Galvanostatic charge-discharge measurements
42
43 were performed at 1 A g^{-1} and corresponding capacitances were calculated from the slopes of the
44
45 curves. Gravimetric capacitances were calculated from the total mass of the composite electrode;
46
47 associated volumetric capacitances were obtained using the density of the respective electrodes.
48
49 Electrochemical impedance spectroscopy (EIS) was performed between 100 mHz and 200 kHz
50
51 in two-electrode configuration after polarization at 0.5 V vs. Ag using a three-electrode setup.
52
53
54
55
56
57
58
59
60
61
62
63
64
65

2.3 Material characterization

A scanning electron microscope (SEM, JSM-6700F, JEOL) was used to investigate the electrodes' morphology and structure. X-ray diffraction (XRD) patterns of the CNT-Ti₃C₂ electrodes were collected by a Bruker D8 diffractometer using a Cu K_α radiation ($\lambda=1.5406 \text{ \AA}$) in the range $2\theta=5\text{--}50^\circ$ with a step of 0.016° . The samples were polarized at different potentials using a 2-electrode cell (LRCS, University de Picardie Jules Verne, Amiens, France) covered with a beryllium window served as the current collector, avoiding electrolyte evaporation and allowing *in situ* electrochemical XRD. Nitrogen sorption analysis at 77 K using Micromeritics ASAP 2020 apparatus was carried out for calculating the specific surface area (SSA) using the Brunauer–Emmet–Teller (BET) equation after outgassing under vacuum at 300 °C for 12 h.”

3. Results and discussion

Figure 1 shows cross-section SEM images of electrode materials. The as-prepared MXene clay, denoted as Ti₃C₂T_x, is shown in Figure 1a. MXene layers can be rolled and sheared, forming a freestanding flexible electrode [20, 21]. Fully delaminated MXene electrodes, denoted as d-Ti₃C₂T_x (Figure 1b), were prepared for improving the electrochemical performance by taking advantage of a higher specific surface area (SSA) resulting from delamination. The SSA values were 23 m² g⁻¹ for multilayered Ti₃C₂ and 98 m² g⁻¹ for delaminated Ti₃C₂ measured elsewhere by nitrogen gas sorption analysis [12]. However, previous studies demonstrated that restacking of delaminated MXene layers forming a dense MXene “paper” with in-plane alignment of MXene sheets limits the accessibility of electrolyte ions. Such restacking issue can be prevented by addition of carbon nanoparticles [14, 22]. Accordingly, composite electrodes were prepared

1
2
3
4 by mixing appropriate amounts of d-Ti₃C₂T_x and MWCNTs. The SSA obtained by nitrogen gas
5 sorption analysis was 70 m² g⁻¹ for the CNT-Ti₃C₂T_x. Figure 1c-d show SEM images of a cross-
6 section of the CNT-Ti₃C₂T_x composite electrode, where CNTs are homogeneously spread
7 between the Ti₃C₂ layers since no aggregates can be seen. Aside preventing restacking, CNT
8 addition is known to increase the conductivity of the electrodes [14, 22, 25-27].
9

10
11
12
13
14
15
16 Figure 2 shows cyclic voltammograms (CVs) of the three Ti₃C₂-based electrodes at 20 mV s⁻¹
17 in 1M EMITFSI in acetonitrile. The electrochemical signatures of the three samples appear to be
18 similar, characterized by a capacitive envelope and a set of redox peaks around -0.2 V and -0.4 V
19 vs. Ag. The potential difference between the oxidation and the reduction peaks, associated with
20 kinetics and ohmic limitations, changes from one electrode to another. The smaller difference is
21 observed for CNT-Ti₃C₂T_x that can be associated in a first approach to a faster diffusion path,
22 thanks to the addition of CNTs. Ti₃C₂T_x shows similar electrochemical signature with a slightly
23 larger overpotential and d-Ti₃C₂T_x shows the largest overpotential and more resistive behavior,
24 possibly due to the restacking of delaminated layers during electrode preparation. The potential
25 range (1.8 V) is narrower than expected from this electrolyte, but could be explained by water
26 trapped between Ti₃C₂ layers, responsible for electrolyte reaction at the extrema of the potential
27 range visible at low scan rates.
28
29
30
31
32
33
34
35
36
37
38
39
40
41
42
43
44
45

46
47 The change of the capacitance (calculated from the integration of the charge during CV
48 measurements) with the potential scan rate is shown Figure 2d. Capacitance up to 245 F cm⁻³ (85
49 F g⁻¹) was obtained at 2 mV s⁻¹ for CNT-Ti₃C₂, with 75% capacitance retention at 100 mV s⁻¹
50 (50% for d-Ti₃C₂T_x). This performance highlights a fairly high power capability of the
51 electrodes, which is assumed to originate from the open 2D structure of the material and the
52
53
54
55
56
57
58
59
60
61
62
63
64
65

1
2
3
4 associated high accessibility of the surface to ions. The lower rate performance of d-Ti₃C₂ could
5
6 be attributed to poor charge percolation.
7
8

9
10 The electrochemical impedance spectroscopy measurements (Figure 3) on the three different
11
12 samples at a bias voltage of 0.5 V (OCV) suggest that the addition of MWCNT greatly improves
13
14 the charge percolation of the electrode. Additionally, there is little to no influence of MWCNTs
15
16 on the electronic conductivity of the electrode, as can be seen from the constant value of the
17
18 high-frequency resistance. This can be explained by a much higher conductivity of metallic
19
20 Ti₃C₂T_x electrode films (~ 2000 S cm⁻¹ [28]) compared to conventional activated carbon, oxide
21
22 or even graphene electrodes.
23
24
25
26

27
28 Figure 4a-c shows the galvanostatic charge-discharge curves obtained at 1A g⁻¹ of the three
29
30 electrodes. The curves are almost linear but contain a slight change in their slopes which
31
32 correspond to the redox peaks identified previously. It appears that the electrodes exhibit pseudo-
33
34 capacitive behavior. Also, a 5-10 times lower specific surface area of MXene [19] compared to
35
36 activated carbons [4] would lead to a very low capacitance without contribution of charge-
37
38 transfer processes. Figure 4d shows the cycle life for the different electrodes, at 1A g⁻¹. CNT-
39
40 Ti₃C₂T_x shows a good stability, with 90% capacitance retention after 1,000 cycles. Ti₃C₂T_x and
41
42 d-Ti₃C₂T_x show a lower stability and faster capacitance decrease during cycling, as well as a
43
44 lower coulombic efficiency.
45
46
47
48
49

50
51 The energy storage mechanism was investigated by recording *in situ* XRD patterns at different
52
53 potentials (Figure 5a). The comparison of patterns indicates that depending on the applied
54
55 potential two different sets of Bragg peaks are observed and that the phase change occurs at the
56
57 same potential where the set of redox peaks appears in the CV (Fig. 2c). This shows that
58
59
60
61
62
63
64
65

1
2
3
4 intercalation/deintercalation processes follow a reversible two-phase mechanism, which differs
5
6 from the progressive and continuous intercalation process previously observed for MXenes
7
8 materials in aqueous supercapacitor [19] and metal-ions capacitors [16,17]. Each set of Bragg
9
10 peaks can be indexed, in agreement with *Ghidu et al* [20], using the (00l) diffraction planes of
11
12 Ti_3C_2 which are characteristic of the interlayer space. On the basis of the diffraction angle of
13
14 (002) Bragg peaks (fig. 5b), it can be deduced that in the -0.8 V to -0.5 V potential range, the
15
16 interlayer distance is 1.3 Å larger than at potentials above -0.5 V and should correspond to the
17
18 intercalation and de-intercalation of ions from the electrolyte into $Ti_3C_2T_x$.
19
20
21
22
23

24
25 Considering the low value of the intercalation potential, one can assume in a first
26
27 approximation that the expansion is due to the intercalation of the EMI^+ cations between Ti_3C_2
28
29 layers and the shrinkage is attributed to its de-intercalation. Reversible intercalation of organic
30
31 ions accompanied by peaks in CVs was observed for porous carbon electrodes, when the ion size
32
33 was somewhat larger than the pore size [29]. Interestingly when cycled within the 0.1 V to 1 V
34
35 potential range, $Ti_3C_2T_x$ capacitance quickly decreases with the cycle number, while it is more
36
37 stable when cycled between -0.8 V and 0.1 V, as shown Figure 6. This suggests that the
38
39 capacitive behavior observed above 0 V is associated with a redox process at negative potentials.
40
41 In other 2D materials, it is admitted that the intercalation of ions can form a pillared structure
42
43 [18, 30-32]. It is possible that cycling exclusively in the positive region causes the structure to
44
45 collapse.
46
47
48
49
50

51
52 Further evidence that the redox reaction is due to the intercalation of cations is provided by
53
54 comparison of the CVs of CNT- $Ti_3C_2T_x$ in 1M solutions of EMITFSI, EMIBF₄ and TEABF₄ in
55
56 acetonitrile. Figure 7a shows the CV of the CNT- $Ti_3C_2T_x$ electrode in 1 M EMIBF₄ in
57
58 acetonitrile electrolyte (a smaller anion but the same cation as in Figure 2). The electrochemical
59
60
61
62
63
64
65

signature is similar to that obtained in 1M EMITFSI in acetonitrile electrolyte (Figure 2); more specifically, we note the presence of a set of redox peaks at the same potential. Figure 7b shows the CV of the CNT-Ti₃C₂T_x electrode in 1 M TEABF₄ in acetonitrile electrolyte. When replacing the “planar” EMI⁺ cation with the larger and more “spherical” TEA⁺ cation, the electrochemical response is drastically changed. The reduction (intercalation) peak is present at a lower potential (-1 V vs Ag wire), but the reaction seems irreversible with an oxidation wave shifted to about 0.5 V. Probably, large TEA⁺ ions are stuck between MXene sheets after intercalation, decreasing the reversibility of the process, but also contributing to pillaring. These measurements suggest that the intercalation/deintercalation of the EMI⁺ cation is responsible for the reversible redox process occurring at -0.4 V vs. Ag. This hypothesis should be further confirmed by other *in situ* characterization techniques, such as electrochemical quartz crystal microbalance [33] or nuclear magnetic resonance [34].

4. Conclusions

The electrochemical behavior of Ti₃C₂T_x as an electrochemical capacitor electrode in organic electrolytes has been investigated. Capacitance up to 32 F g⁻¹ was obtained for as-produced Ti₃C₂T_x MXene clay and improved to 85 F g⁻¹ by delamination and addition of carbon nanotubes. Intercalation of large EMI⁺ cations between the layers of Ti₃C₂ has been demonstrated suggesting that other large or multivalent cations may be similarly intercalated into MXenes from organic electrolyte solutions. Ti₃C₂T_x capacitance was increased 3-fold, up to 85 F g⁻¹ and 245 F cm⁻³ at 2 mV s⁻¹ by using carbon nanotubes as an additive to improve ion accessibility to the active material. The CNT/Ti₃C₂T_x electrodes show a good rate performance and good cycle life stability. Considering that this is the first report on capacitance of Ti₃C₂ in organic electrolytes used in supercapacitors and that Ti₃C₂ is only one of more than a dozen of

1
2
3
4 already synthesized MXenes, there are good reasons to expect further improvement in
5
6 capacitance as the optimal MXene-electrolyte couples have been identified and their
7
8 performance optimized. It took less than two years to increase capacitance of Ti₃C₂-MXene in
9
10 aqueous electrolyte from about 100 F g⁻¹ [19] to 320 F g⁻¹ [21] and we expect fast improvement
11
12 of capacitance in organic electrolytes as well.
13
14

15 16 **ACKNOWLEDGEMENT**

17
18 We thank C. E. Ren for help with material synthesis, Kathleen Maleski for comments on the
19
20 manuscript (both, Drexel University), B. Daffos for the SEM images and gas sorption analysis,
21
22 and B. Duployer for help in *in situ* XRD experiments (both, Université Paul Sabatier). This work
23
24 was supported by the Partnership Universities Fund (PUF) of French Embassy. YDA was
25
26 supported by the European Research Council (ERC, Advanced Grant, ERC-2011-AdG, Project
27
28 291543 – IONACES). PS acknowledges the funding from the Chair of Excellence of the Airbus
29
30 group foundation “Embedded multi-functional materials”.
31
32
33
34
35

36 37 **REFERENCES**

- 38
39 [1] M. Armand, J.M. Tarascon, *Nature*, 451 (2008) 652-657.
40 [2] J.R. Miller, P. Simon, *Science*, 321 (2008) 651-652.
41 [3] L.L. Zhang, X.S. Zhao, *Chemical Society Reviews*, 38 (2009) 2520-2531.
42 [4] P. Simon, Y. Gogotsi, *Nat. Mater.*, 7 (2008) 845-854.
43 [5] J.P. Zheng, P.J. Cygan, T.R. Jow, *J. Electrochem. Soc.*, 142 (1995) 2699-2703.
44 [6] H.Y. Lee, J.B. Goodenough, *J. Solid State Chem.*, 144 (1999) 220-223.
45 [7] V. Augustyn, P. Simon, B. Dunn, *Energy & Environmental Science*, 7 (2014) 1597-1614.
46 [8] X. Xiao, C. Zhang, S. Lin, L. Huang, Z. Hu, Y. Cheng, T. Li, W. Qiao, D. Long, Y. Huang,
47 L. Mai, Y. Gogotsi, J. Zhou, *Energy Storage Materials*, 1 (2015) 1-8.
48 [9] Y. Zhu, S. Murali, M.D. Stoller, K.J. Ganesh, W. Cai, P.J. Ferreira, A. Pirkle, R.M. Wallace,
49 K.A. Cychoz, M. Thommes, D. Su, E.A. Stach, R.S. Ruoff, *Science*, 332 (2011) 1537-1541.
50 [10] Z. Fan, J. Yan, L. Zhi, Q. Zhang, T. Wei, J. Feng, M. Zhang, W. Qian, F. Wei, *Adv. Mater.*,
51 22 (2010) 3723-3728.
52 [11] M. Naguib, J. Come, B. Dyatkin, V. Presser, P.-L. Taberna, P. Simon, M.W. Barsoum, Y.
53 Gogotsi, *Electrochemistry Communications*, 16 (2012) 61-64.
54 [12] O. Mashtalir, M. Naguib, V.N. Mochalin, Y. Dall’Agnese, M. Heon, M.W. Barsoum, Y.
55 Gogotsi, *Nat Commun*, 4 (2013) 1716.
56
57
58
59
60
61
62
63
64
65

- 1
2
3
4 [13] Y. Xie, Y. Dall'Agnesse, M. Naguib, Y. Gogotsi, M.W. Barsoum, H.L. Zhuang, P.R.C. Kent,
5 ACS Nano, 8 (2014) 9606-9615.
6 [14] Y. Liu, W. Wang, Y. Ying, Y. Wang, X. Peng, Dalton Trans., 44 (2015) 7123-7126.
7 [15] M. Naguib, J. Halim, J. Lu, K.M. Cook, L. Hultman, Y. Gogotsi, M.W. Barsoum, Journal of
8 the American Chemical Society, 135 (2013) 15966-15969.
9 [16] J. Come, M. Naguib, P. Rozier, M.W. Barsoum, Y. Gogotsi, P.L. Taberna, M. Morcrette, P.
10 Simon, J. Electrochem. Soc., 159 (2012) A1368-A1373.
11 [17] Y. Dall'Agnesse, P.-L. Taberna, Y. Gogotsi, P. Simon, The Journal of Physical Chemistry
12 Letters, 6 (2015) 2305-2309.
13 [18] X. Wang, S. Kajiyama, H. Iinuma, E. Hosono, S. Oro, I. Moriguchi, M. Okubo, A. Yamada,
14 Nat Commun, 6 (2015).
15 [19] M.R. Lukatskaya, O. Mashtalir, C.E. Ren, Y. Dall'Agnesse, P. Rozier, P.L. Taberna, M.
16 Naguib, P. Simon, M.W. Barsoum, Y. Gogotsi, Science, 341 (2013) 1502-1505.
17 [20] M. Ghidui, M.R. Lukatskaya, M.-Q. Zhao, Y. Gogotsi, M.W. Barsoum, Nature, 516 (2014)
18 78-81.
19 [21] Y. Dall'Agnesse, M.R. Lukatskaya, K.M. Cook, P.-L. Taberna, Y. Gogotsi, P. Simon,
20 Electrochemistry Communications, 48 (2014) 118-122.
21 [22] M.-Q. Zhao, C.E. Ren, Z. Ling, M.R. Lukatskaya, C. Zhang, K.L. Van Aken, M.W.
22 Barsoum, Y. Gogotsi, Advanced Materials, 27 (2015) 339-345.
23 [23] M. Naguib, Y. Gogotsi, Accounts of Chemical Research, 48 (2015) 128-135.
24 [24] M.R. Lukatskaya, S.-M. Bak, X. Yu, X.-Q. Yang, M.W. Barsoum, Y. Gogotsi, Advanced
25 Energy Materials, 5 (2015) 1500589.
26 [25] Q. Cheng, J. Tang, J. Ma, H. Zhang, N. Shinya, L.-C. Qin, Phys. Chem. Chem. Phys., 13
27 (2011) 17615-17624.
28 [26] X.-M. Liu, Z.d. Huang, S.w. Oh, B. Zhang, P.-C. Ma, M.M.F. Yuen, J.-K. Kim, Composites
29 Science and Technology, 72 (2012) 121-144.
30 [27] B.J. Landi, M.J. Ganter, C.D. Cress, R.A. DiLeo, R.P. Raffaele, Energy & Environmental
31 Science, 2 (2009) 638-654.
32 [28] Z. Ling, C.E. Ren, M.-Q. Zhao, J. Yang, J.M. Giammarco, J. Qiu, M.W. Barsoum, Y.
33 Gogotsi, Proceedings of the National Academy of Sciences, 111 (2014) 16676-16681.
34 [29] R. Lin, P. Huang, J. Ségalini, C. Largeot, P.L. Taberna, J. Chmiola, Y. Gogotsi, P. Simon,
35 Electrochimica Acta, 54 (2009) 7025-7032.
36 [30] M.M. Hantel, R. Nesper, A. Wokaun, R. Kötz, Electrochimica Acta, 134 (2014) 459-470.
37 [31] Y. Dong, X. Xu, S. Li, C. Han, K. Zhao, L. Zhang, C. Niu, Z. Huang, L. Mai, Nano Energy,
38 15 (2015) 145-152.
39 [32] H. Li, G. Zhu, Z. Yang, Z. Wang, Z.-H. Liu, J. Colloid Interface Sci., 345 (2010) 228-233.
40 [33] M.D. Levi, M.R. Lukatskaya, S. Sigalov, M. Beidaghi, N. Shpigel, L. Daikhin, D. Aurbach,
41 M.W. Barsoum, Y. Gogotsi, Advanced Energy Materials, 5 (2015) 1400815.
42 [34] J.M. Griffin, A.C. Forse, W.-Y. Tsai, P.-L. Taberna, P. Simon, C.P. Grey, Nat Mater, 14
43 (2015) 812-819.
44
45
46
47
48
49
50
51
52
53
54
55
56
57
58
59
60
61
62
63
64
65

Figure 1
[Click here to download high resolution image](#)

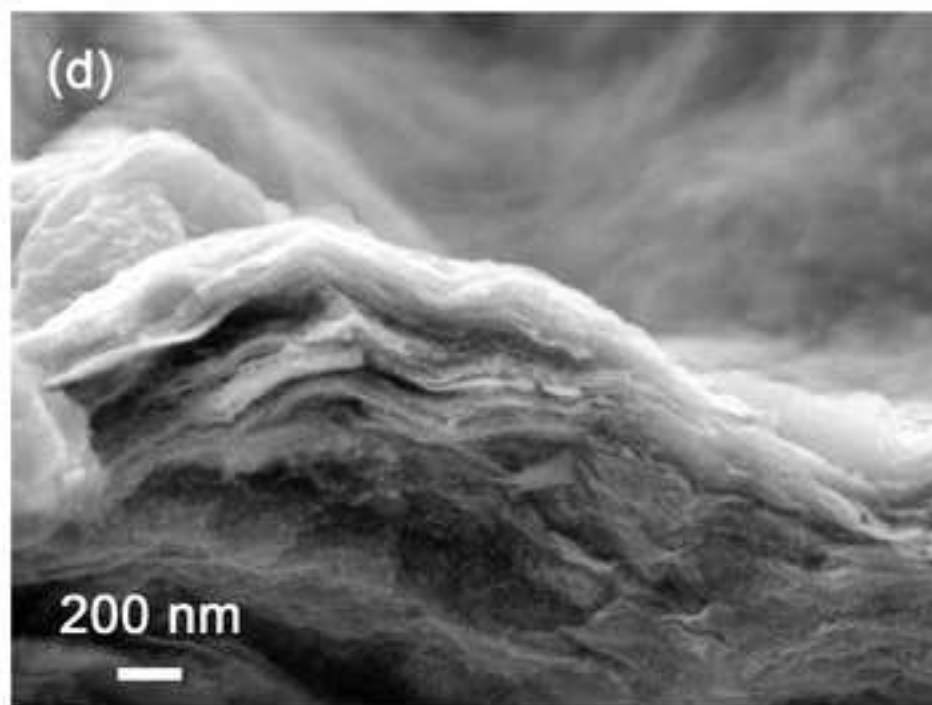
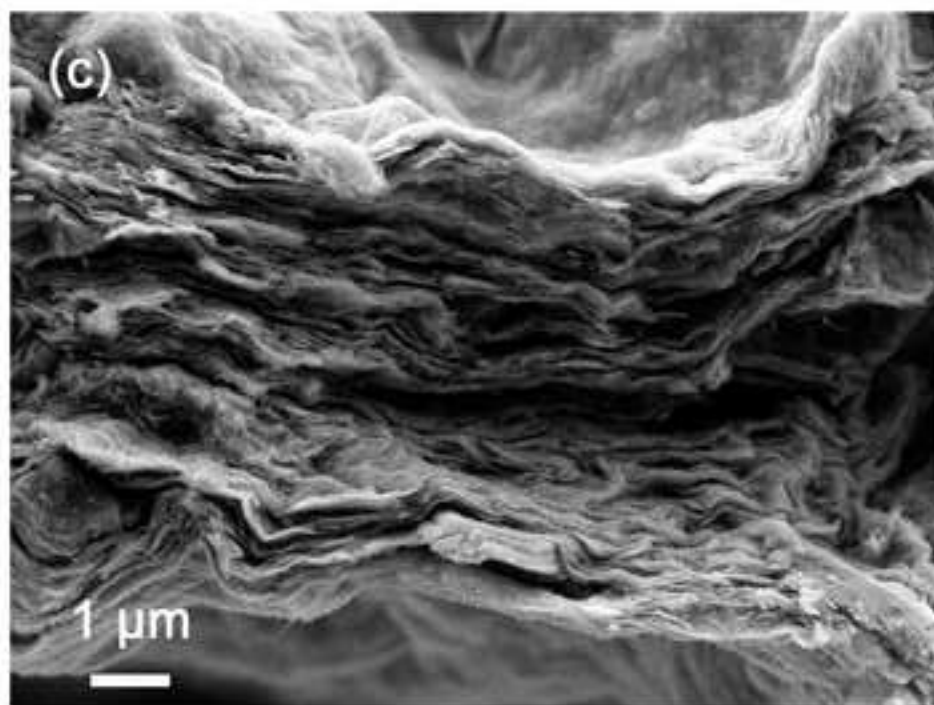
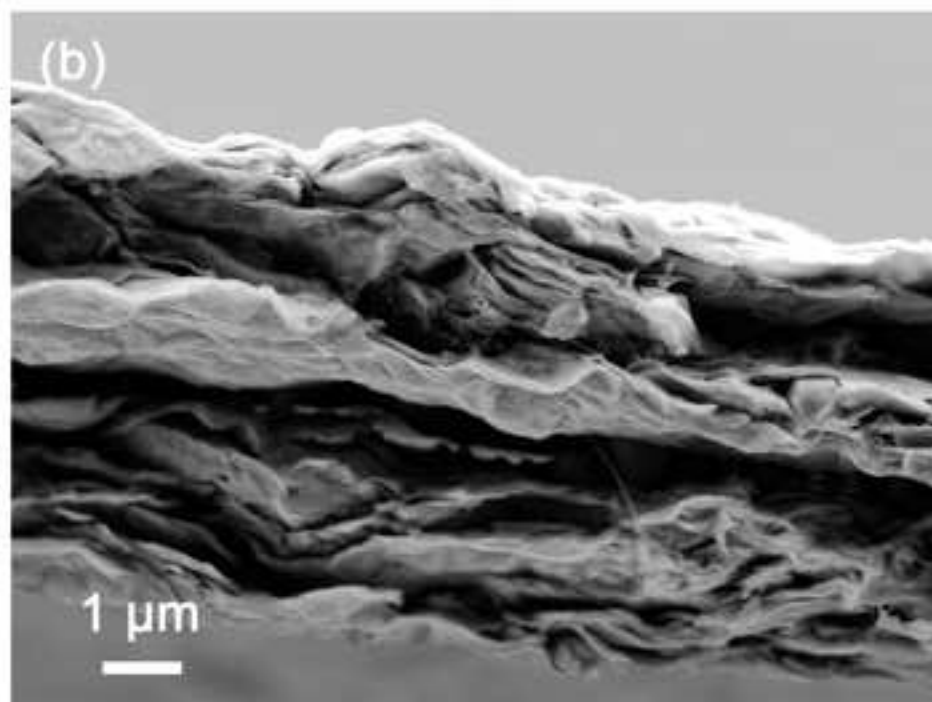
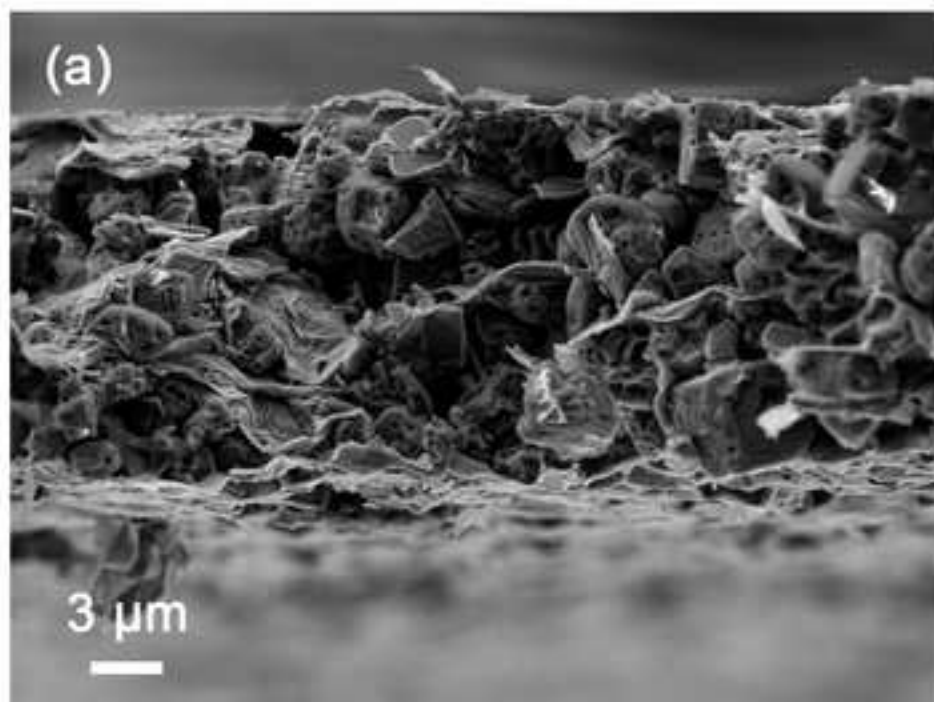


Figure 2
[Click here to download high resolution image](#)

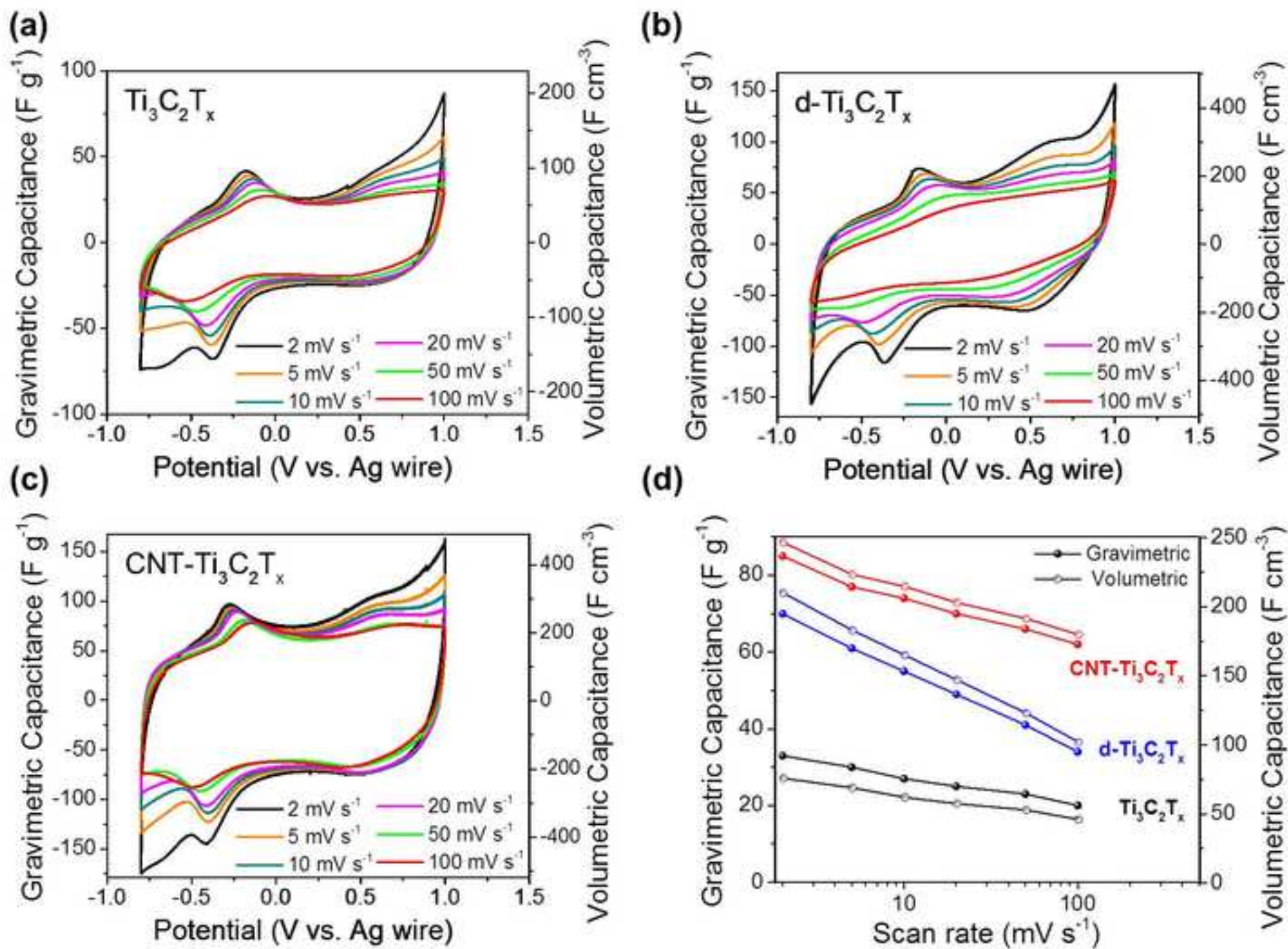


Figure 3
[Click here to download high resolution image](#)

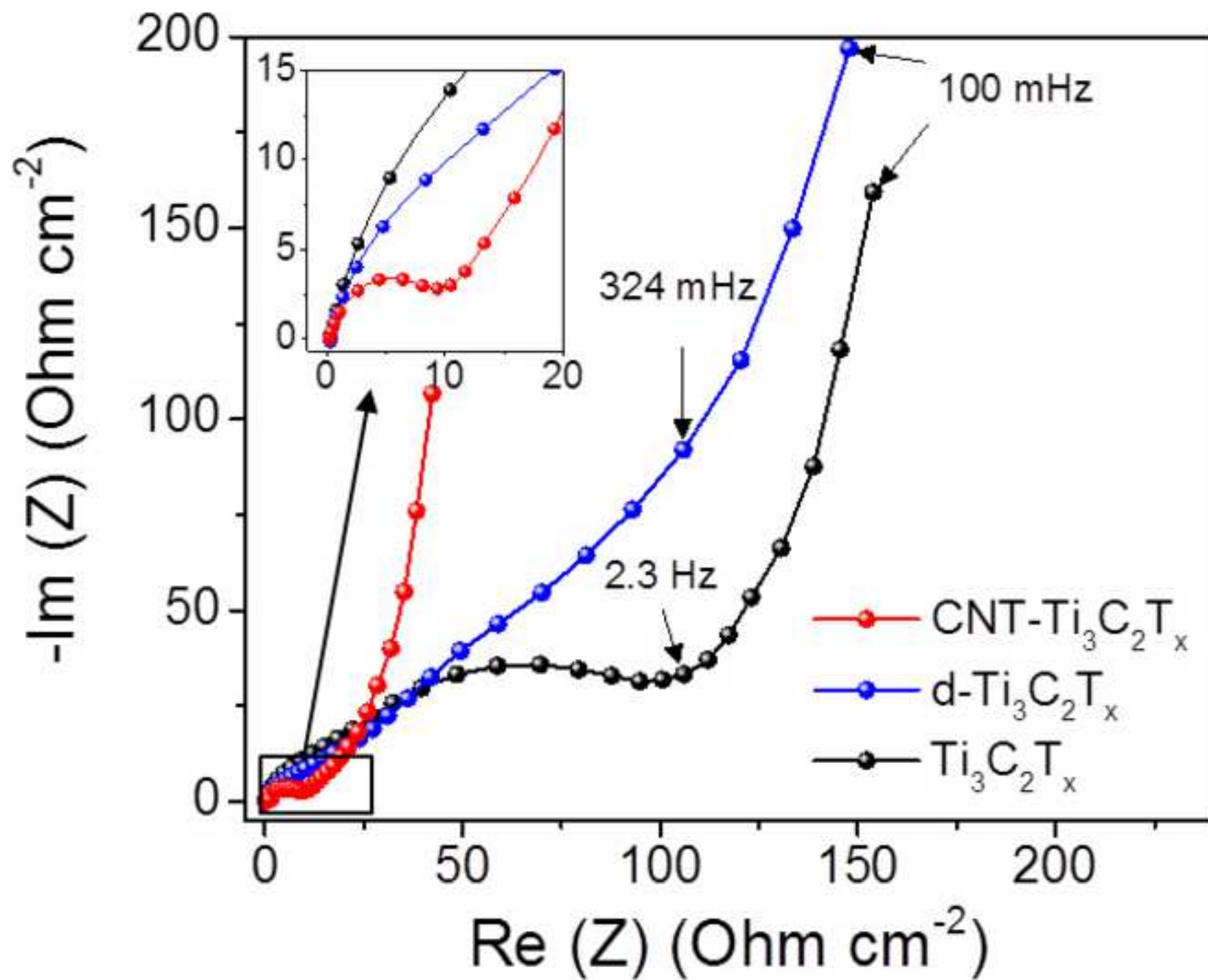


Figure 4
[Click here to download high resolution image](#)

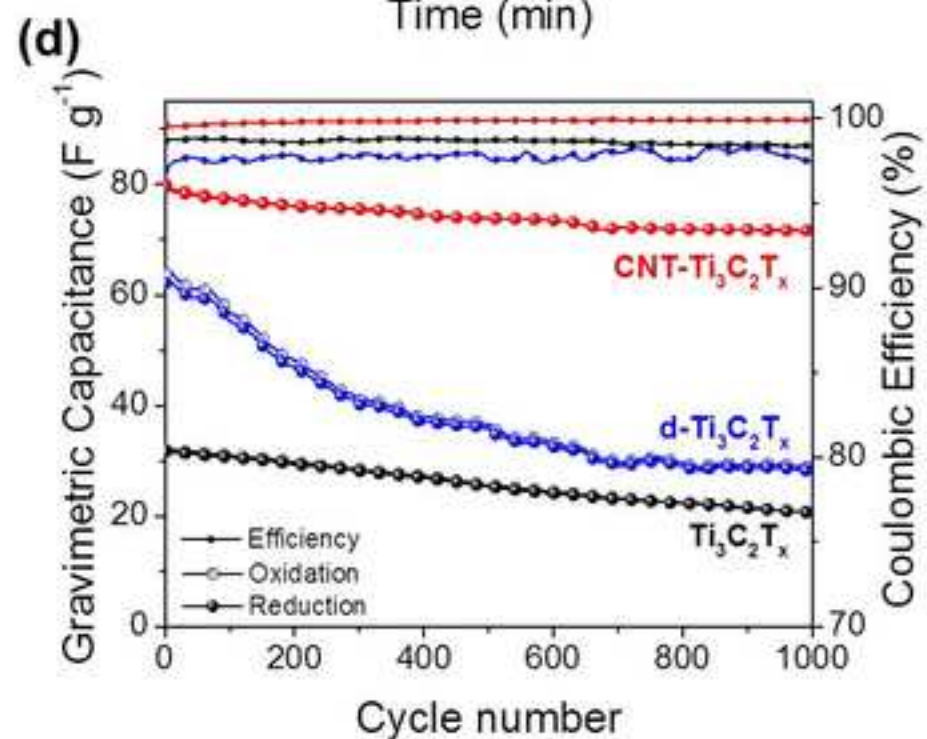
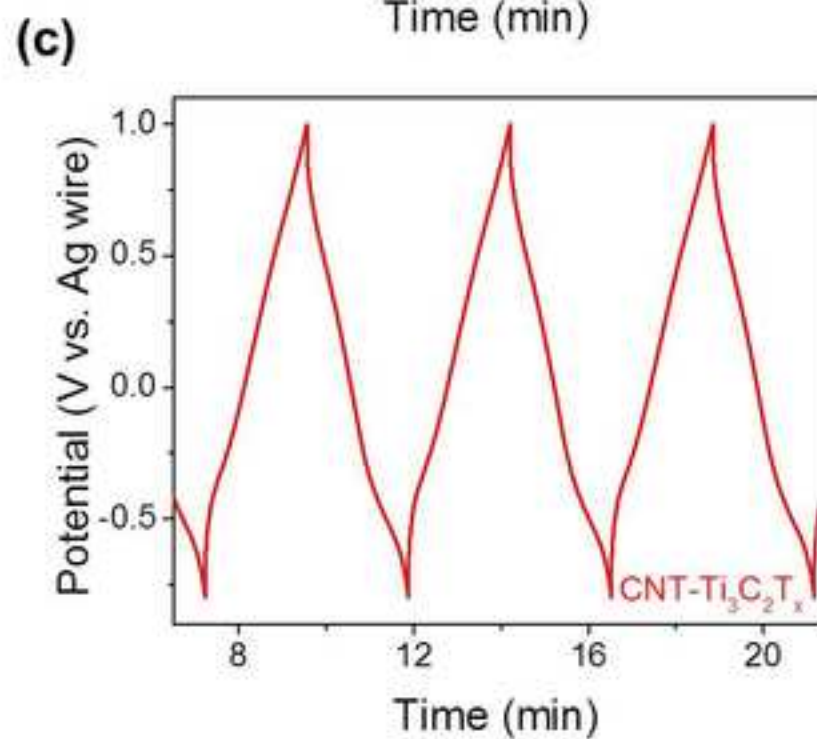
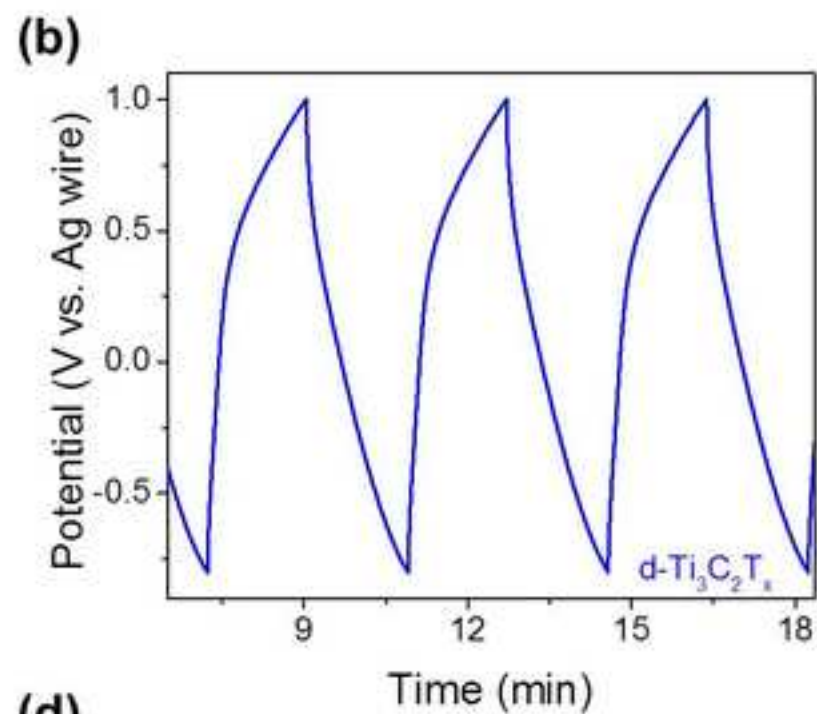
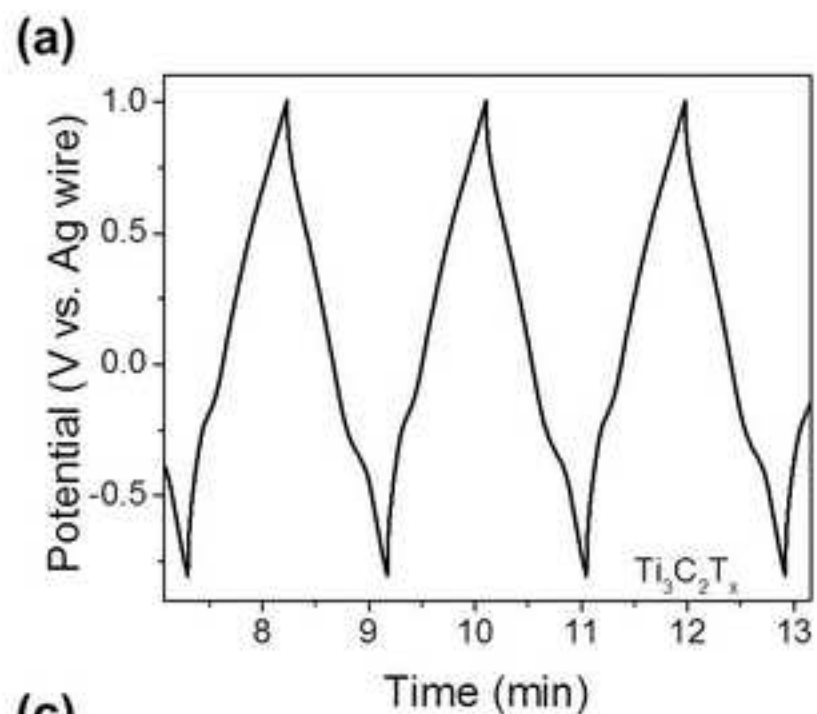


Figure 5
[Click here to download high resolution image](#)

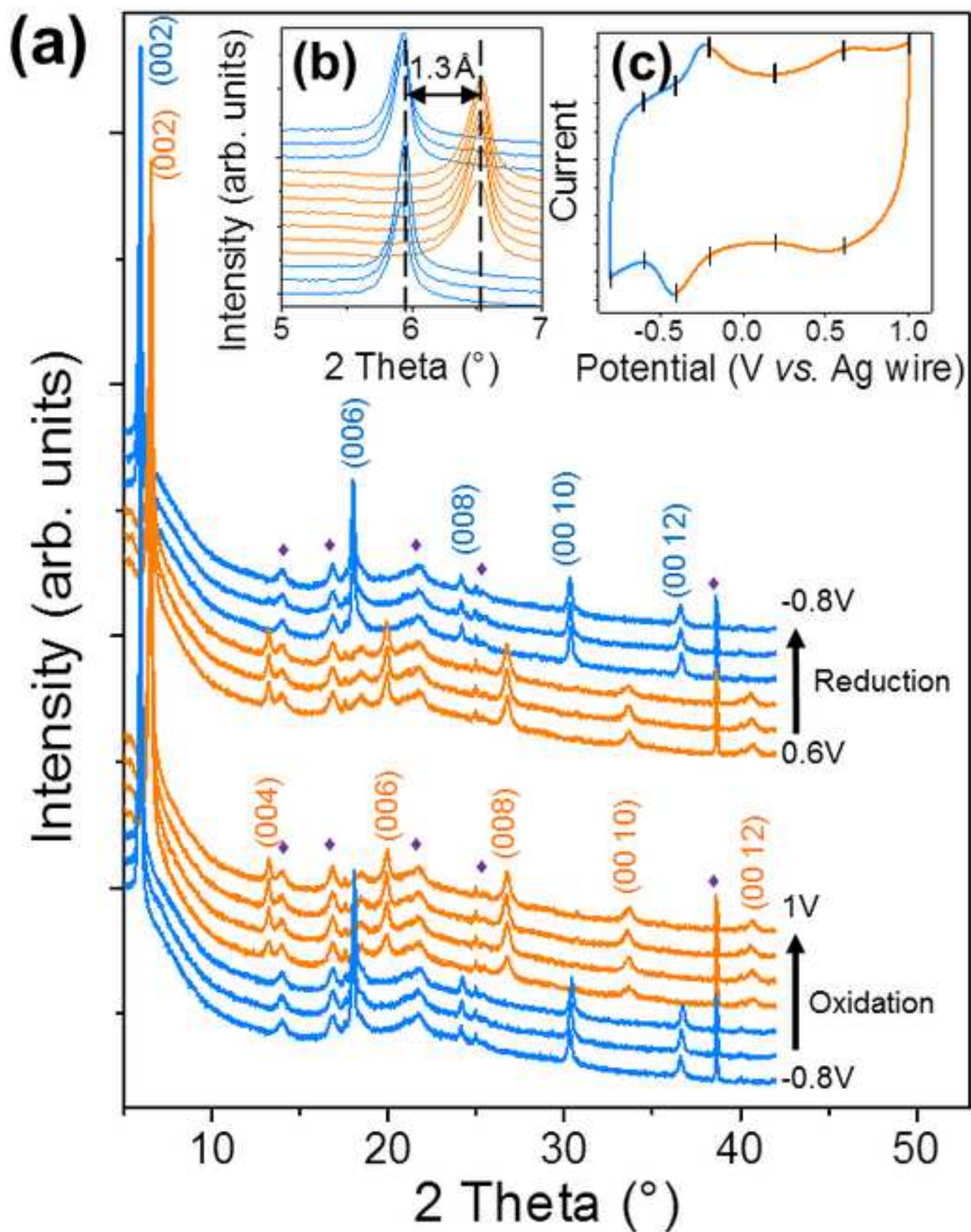


Figure 6
[Click here to download high resolution image](#)

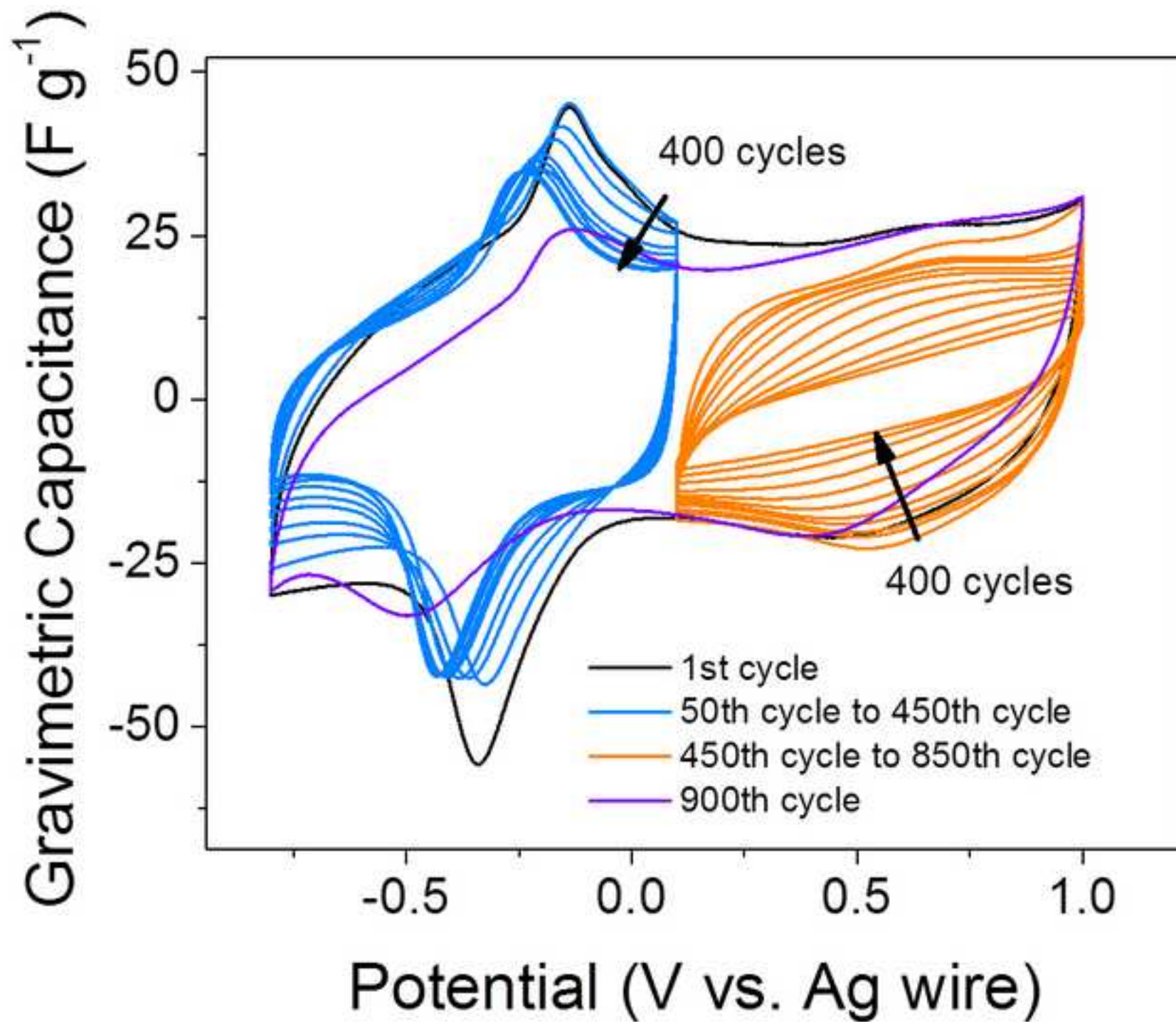


Figure 7

[Click here to download high resolution image](#)

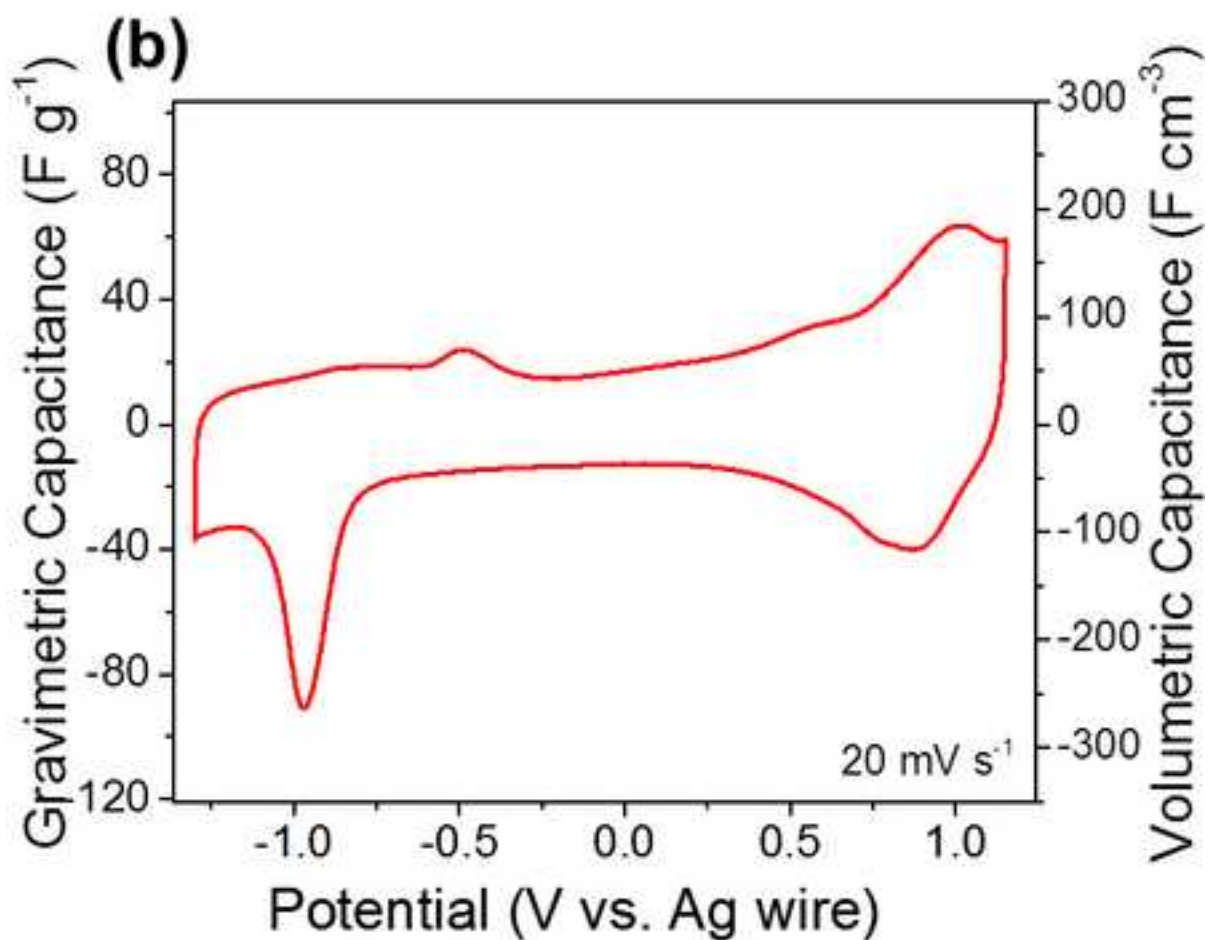
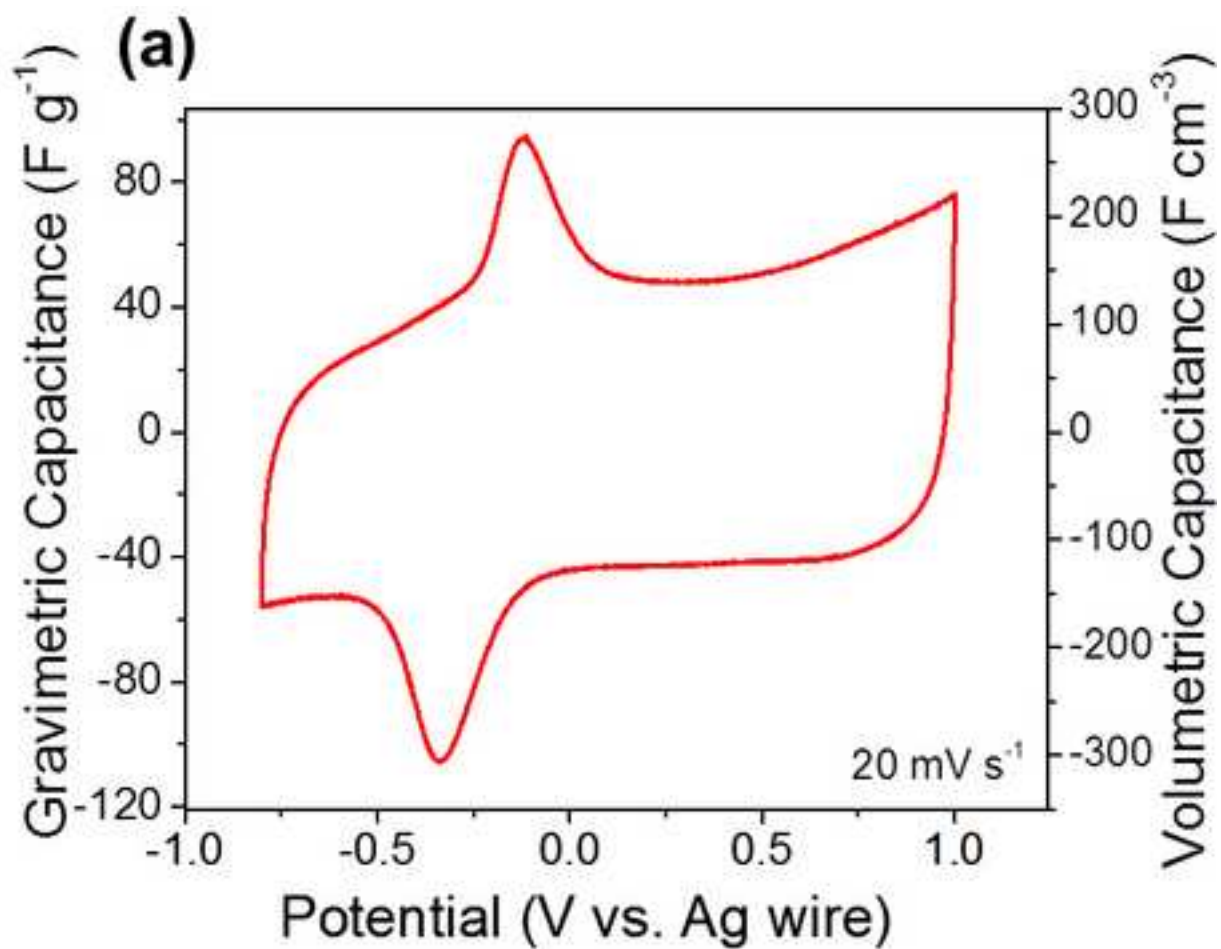


Figure 1. Scanning electron microscope images of (a) rolled $\text{Ti}_3\text{C}_2\text{T}_x$ “clay”, (b) d- $\text{Ti}_3\text{C}_2\text{T}_x$ and (c-d) CNT- $\text{Ti}_3\text{C}_2\text{T}_x$ electrode films.

Figure 2. Cyclic voltammograms of (a) $\text{Ti}_3\text{C}_2\text{T}_x$, (b) d- $\text{Ti}_3\text{C}_2\text{T}_x$ and (c) CNT- $\text{Ti}_3\text{C}_2\text{T}_x$ in 1M EMITFSI in acetonitrile electrolyte at different scan rates and (d) summary of the change of capacitance with the potential scan rate. These measurements were done using a three-electrode Swagelok cell.

Figure 3. Nyquist plot at 0.5 V vs. Ag reference obtained using a two-electrode setup.

Figure 4. Galvanostatic charge-discharge curves of (a) $\text{Ti}_3\text{C}_2\text{T}_x$, (b) d- $\text{Ti}_3\text{C}_2\text{T}_x$ and (c) CNT- $\text{Ti}_3\text{C}_2\text{T}_x$ in 1M EMITFSI in acetonitrile electrolyte obtained at 1 A g^{-1} and (d) the corresponding cycle life of those electrodes. These measurements were done using a three-electrode Swagelok cell.

Figure 5: In-situ XRD patterns of CNT- $\text{Ti}_3\text{C}_2\text{T}_x$ at different potentials in the $5\text{-}50^\circ$ 2θ range. Purple diamonds indicate peaks coming from the cell for *in situ* measurements. Inset (b) shows a zoom in the $5\text{-}7^\circ$ 2θ range and (c) CV recorded at 20 mV s^{-1} .

Figure 6. Cyclic voltammograms of $\text{Ti}_3\text{C}_2\text{T}_x$ in different potential ranges at 20 mV s^{-1} .

Figure 7. Cyclic voltammetry of CNT- $\text{Ti}_3\text{C}_2\text{T}_x$ at 20 mV s^{-1} in 1 M solutions of EMIBF₄ (a) and TEABF₄ in acetonitrile (b).